symmetry

MDPI

Article

Determining the Impact of High Temperature Fire Conditions on Fibre Cement Boards Using Thermogravimetric Analysis

Tomas Veliseicik [1], Ramune Zurauskiene [1] and Marina Valentukeviciene [2,*]

[1] Faculty of Civil Engineering, Vilnius Gediminas Technical University, Vilnius LT10223, Lithuania; tomas.veliseicik@vgtu.lt (T.V.); ramune.zurauskiene@vgtu.lt (R.Z.)
[2] Faculty of Environmental Engineering, Vilnius Gediminas Technical University, Vilnius LT10223, Lithuania
* Correspondence: marina.valentukeviciene@vgtu.lt; Tel.: +370-616-53746

Received: 21 September 2020; Accepted: 16 October 2020; Published: 18 October 2020

Abstract: When exposed to temperatures that are progressively and rapidly raised, large dimension fibre cement boards tend to crack. This occurrence is analysed and explained for a specific issue of asymmetric growth of a curvilinear crack in high temperatures. This phenomenon occurred while performing Single Burning Item (SBI) experiments at fire loads which are higher than those used in countries of the European Union, which better reflect fire events that may occur in high-rise buildings. In such conditions, fibre cement boards crack, allowing the fire to reach the thermal insulating material which then combusts, thereby helping to spread the conflagration to upper floors. This experiment investigated the temperatures at which fibre cement boards crack, and why. Thermal analysis methods and thermogravimetric experiments were conducted on the fibre boards, followed by x-ray phase analysis investigations. During this phase, x-ray structural analysis was performed while the fibre cement was exposed to temperatures of 1000 °C. The article also presents ongoing change results when heating only composite fibre-cement board materials; phase changes that take place in high temperatures are discussed.

Keywords: fibre-cement; ventilated facade; explosive destruction; thermogravimetric analysis; X-ray phase analysis in high temperature

1. Introduction

Composite materials fall into two main categories, matrix and dispersion [1], each of which has different functions and characteristics. A composite material is defined as having a compound different phase property function; the most notable influence is present in the dispersion phase. Fibre-cement is one such composite and belongs in the matrix group. The use of composites—a combination of at least two different types of material—in building has experienced huge growth in recent years. Due to its great technical properties, fibre-cement in particular is widely used in construction. These plates are flexible, due to which they can be fastened to facade, have high bending strength, have very small shrinkage when dampness changes and are resistant to atmosphere effects [2]. Among other uses, fibre-cement plates are used in inner wall coverage, balcony and terrace enclosure installation, chimney coverage, and roof nailing [3]. They are, however, mainly used for ventilated façade system installations in new building constructions and also renovations. Recent tragic fire events, notably in the UK at London's Grenfell Towers, clearly show that the response of fibre cement under high fire and temperature conditions are crucial, especially where it is a component of ventilated facade installations.

The analysis of publicly available fire causation data shows that 35.5% of fires start in buildings [4]. Due to the recent rise of the use of synthetic polymer material in furniture, household appliances and finishing production, fires spread from the interior of the building to the outside. This phenomenon is of interest to materials scientists who have conducted experiment research, nature-based experiments, mathematical modelling, and analysed flame and fire spreading mechanisms between building floors [5–8]. Inappropriate and/or incorrect facade systems determine how, and how strongly, fire spreads on the exterior surfaces of the building. Not only does this increase the likelihood of deaths due to fire, but also makes it difficult for fire fighters to extinguish the fire and rescue the buildings inhabitants. There is also a high risk of other buildings catching fire, or injury and death to fire fighters. The 2017 Grenfell Tower fire showed how fire can spread from the inside to the exterior (and thereby consuming the entire structure) and has led to the urgent reappraisal of standards and indicators in flammability and fire resistance as they apply to facade systems. To ensure this indicator, these systems must be able to withstand high temperature effect for a certain period of time.

For more than 150 years, it has been known that in the general case, concrete, whose composition contains Portland cement, asymmetric cracks and breaks at high temperatures [9]. For example, the mechanism of concrete thermal cleavage and explosive destruction (disintegration) was first investigated at the end of the nineteenth century and was thoroughly analysed in the twentieth century. More recently, the work of Kristian Hertz has indicated that ultra-strength concrete explosive destruction when heating samples in 1 °C/min speed occurs in the boundaries of 350 °C–650 °C [10]. The explosive destruction (disintegration) of strong concrete was analysed by Phan and Carino who determined that concrete explosions occur in boundaries of 200–325 °C [11]. They found that where concrete is exposed to high temperatures, complicated physicochemical and physic mechanical processes determine its destruction. Firstly, slow capillary water loss and reduction cohesive forces and water expands, beginning the dehydration process of concrete minerals and physically water loss. In higher temperature break up of some siliceous aggregates and reach critical water temperature during that water changes properties, beginning the decomposition of some concrete minerals; also present is thermal expansion of different aggregates [12]. Experimental research has shown that the destructive effect of high temperatures to concrete is usually related to heat, tension, and humidity, which has been the subject of a great deal of study [13]. Phan and Carino's work was also reproduced and confirmed as reliable by other scientists. In fact, research efforts were carried out concurrently in the search for various solutions to lower and/or eliminate the aforementioned asymmetric disintegration [14,15]. Research by Lithuanian scientists raised concrete resistance to fire through the inclusion of various additions [14]. They determined that not only concrete drying temperature treatments, but also drying methods, exercise significant influence on concrete explosive disintegration [15].

Fire experiments conducted on a ventilated facade with fibre-cement plates showed that facade plates split within 10 min from the start of the experiment when temperature reaches about 250 °C. In certain situations, the splitting of fibre-cement plate was accompanied by explosions as fragments of plate broke away [16]. The researcher did not investigate the possible explanation for this event.

Having analysed the existing literature, it is evident that there are no detailed research data on the behaviour of fibre-cement at high temperatures, and neither is the fibre-cement explosive destruction mechanism described. This study examined fibre-cement using thermogravimetric analysis and x-ray phase analysis in high temperature methods by determining composite component behaviour at high temperatures, and by searching for the causal link with the phenomenon of explosive destruction (disintegration).

2. Materials and Methods

Research was carried out using fibre-cement plates. Table 1 shows experimented fibre-cement components (dry components) which are included in the composition of the fibre-cement plate. Water was used for plate formation mass mixing.

Table 1. Fibre-cement plate composition in mass by percentage.

Material	Amount, %
Silica sand M32 and M300	51.06
Portland cement CEM I 42.5N	38.04
Cellulose fibre (2 types)	7.09
Aluminium hydroxide ($AlOH_3$)	2.06
Kaolin	1.76

Silica sand is composed of 99.5% silicon dioxide, 0.5% other admixtures (Al_2O_3, Fe_2O_3, TiO_2, K_2O, CaO). Portland cement CEM I 42.5 N, is produced from 95%–100% clinker and 5%–0% calcium sulphate addition, dehydrate gypsum is often added ($CaSO_4 \cdot H_2O$) (EN 197-1). Portland cement composition is shown in Table 2 [17–19].

Table 2. Portland cement CEM I 42.5 N chemical composition [17–19].

Chemical Composition	Weight Content, %
CaO	60–69
SiO_2	20–22
Al_2O_3	4.7–6.3
Fe_2O_3	1.6–4.4
SO_3	1.8–4.6
MgO	0.7–4.2
K_2O	0.65–0.8
Na_2O	0.11–1.2

Portland cement is mainly composed of four minerals. Their percentage amount is shown in Table 3.

Table 3. Portland cement CEM I 42.5 mineralogical composition [17–19].

Mineral	Amount, %
Tricalcium silicate $3CaO \cdot SiO_2$ (3CS)	40–63
Dicalcium silicate $2CaO \cdot SiO_2$ (2CS)	9–31
Tricalcium aluminate $3CaO \cdot Al_2O_3$ (3CA)	6–14
Tetracalcium aluminium ferrite $4CaO \cdot Al_2O_3 \cdot Fe_2O_3$ (4CAF)	5–13

Quartz sand M300 is ground in a rotary mill until its specific surface reaches 4400 cm^2/g when producing fibre-cement plates. A total of 41.07% of ground sand is added into material mixing equipment. A total of 9.99% of sand M32 (it is smaller and is brought already ground) is also added to this equipment. A total of 2.06% of aluminium hydroxide ($AlOH_3$) is added to the mixing equipment, into which 1.76% of kaolin is added. In a separate technological apparatus, armoured fibre is prepared from two types of cellulose. One type of cellulose fibre is shorter (5.45%), whereas other cellulose fibres (1.64%) take the form of a so-called "hand fan". Prepared water pulp is mixed with doses of dry powder, adding 38.04% of extra Portland cement. Everything is mixed for 5 min, and then placed in a Hatschek machine which forms a plate. In the cutting equipment, still moist soft mass is cut into pieces of the desired size. Cut pieces are collected onto metal trays. Plates are held on the trays for 8 h. The trolleys are then placed in autoclaves where the plates are hardened in for 10–12 h under 10 bars of pressure at 120–140 °C.

The composition of fibre-cement plate chemical was determined, and the main oxide composition is shown in Table 4. These oxides compose 90.36% of the mass of the fibre-cement plate. The mass contains 9.39% additional oxygen which can be compounded with carbon. Other oxides compose only 0.25% of the fibre-cement mass.

Table 4. Fibre-cement plate main oxide chemical composition.

Chemical Composition	Weight Content, %
SiO_2	56.25
CaO	24.02
Al_2O_3	4.71
MgO	1.56
Fe_2O_3	1.534
SO_3	1.31
K_2O	0.61
TiO_2	0.25
Na_2O	0.12

Samples cut from plates were milled with a hand mortar and pestle into powder form in order to guarantee the same granulometry and achieve the smallest possible pieces. The researched material mass fluctuated between 17–21 mg. Before. the experiment samples (Figure 1) were conditioned according to LST EN 13238:2010, the standard requirements for conditioning room when the temperature is 22 °C ± 2 °C and humidity is 50% ± 5%.

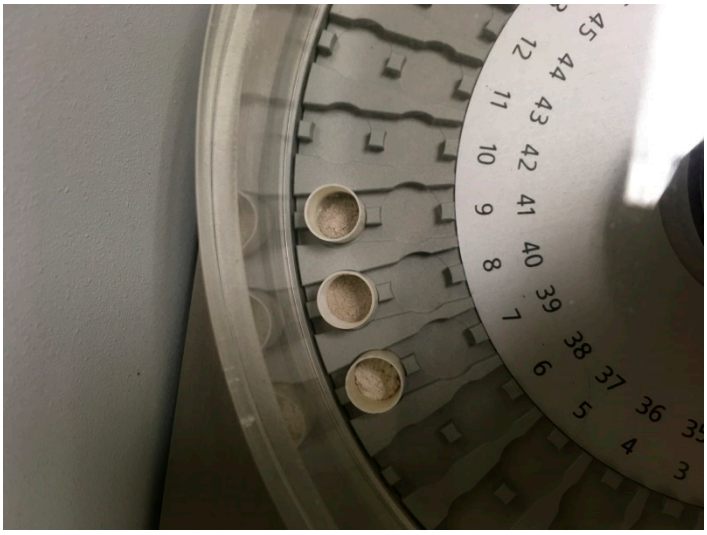

Figure 1. Samples in the thermogravimetric analyser.

Thermogravimetric analysis was performed using a thermogravimetric analyser "NETZSCH TG 209 F1 LIBRA" (Selb, Germany) (Figure 2). The temperature during the experiment was measured with a K type thermocouple using an aluminium oxide (Al_2O_3) crucible with a lid. Thermal analysis was conducted in a nitrogen gas environment guaranteeing a nitrogen debit of 0.04 L/min. Experiments were conducted at temperatures ranging from 35 °C to 1000 °C isotherms. For this heating routine, a rise speed of 10 °C/min temperature was determined. The results are shown in graphs where the abscissa axis shows the respective temperature curve while ordinate axis–thermogravimetric and differential thermogravimetric results.

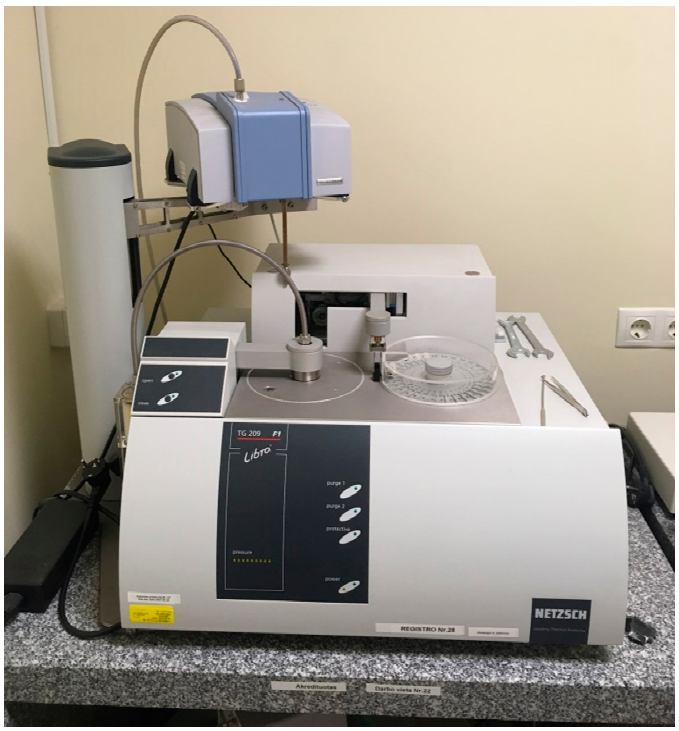

Figure 2. Image of thermogravimetric analyser.

Second and third temperature regimes were chosen in accordance with standard fire curves. The second case had a regime from 35 °C to 680 °C. The rising speed of the temperature was chosen according to the outer fire curve which is defined by this Formula (1) Figure 3.

$$\theta_g = 660(1 - 0.687e^{-0,32t} - 0.313e^{-3,8t}) + 20, \quad (1)$$

where, θ_g–fire temperature (°C), t-time (min).

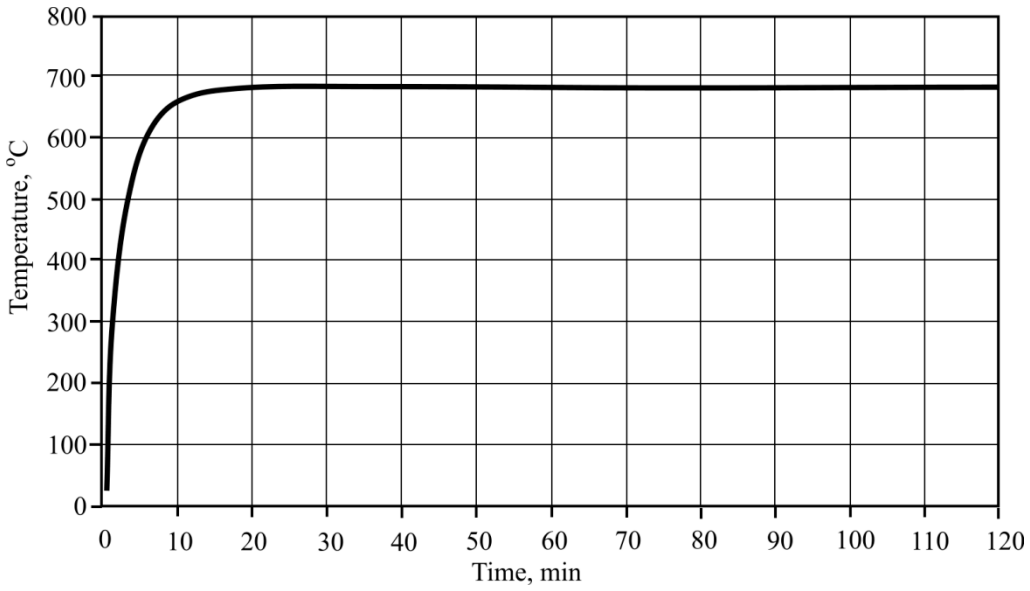

Figure 3. Outer fire curve according Formula 1.

In the third case, the temperature regime was from 35 °C to 842 °C., with the rising speed of the temperature chosen according to the outer fire curve which is defined by this Formula (2) Figure 4.

$$\theta_g = 20 + 345 \log_{10}(8t + 1), \quad (2)$$

where, θ_g–fire temperature (°C), t-time (min).

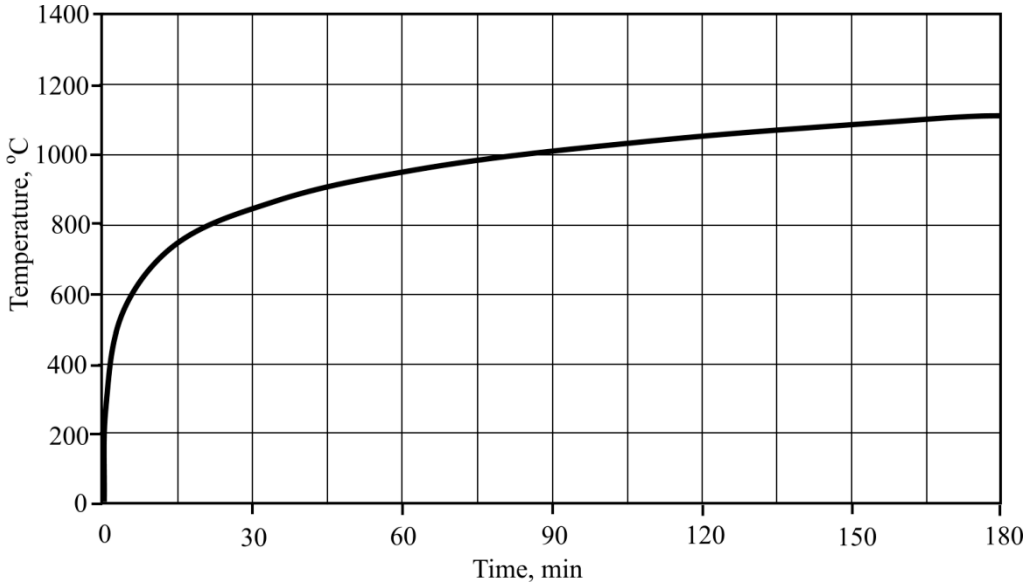

Figure 4. Outer fire curve according Formula 2.

X-ray phase analysis was performed using an X-ray diffractometer (Rigaku, Japan) with a 9 kW X-ray source with spinning Cu anode. The source work regime is Ua = 45 kV, Ia = 200 mA. It was milled with a rotary mill and pressed into 10 mm diameter and 1 mm thickness tablets (vax was not used). A parallel ray fibre X-ray optic was used in order to lower the influence of changes in the thickness of the flat fibre-cement sample during heating towards X-ray accuracy. The fibre-cement sample was analysed in high temperature chamber DHS 1100 (Anton Paar, Graz, Austria). Gas atmosphere temperatures were: 26, 110, 220, 400, 640, 740, 900, and 1000 °C. The analysis was done in a helium gas atmosphere. The speed of the temperature rise is 10 °C/min, and the sample held in the chosen temperature for 10 min before starting to register (measure) the X-ray. X-rays were measured in diffraction corner intervals of 10–60°. The scintillation detector movement speed is 3°/min.

Phase (mineral) identification was done using polycrystalline X-ray processing and analysing program equipment PDXL-2 (Rigaku) (Figure 5), and the international ICDD (International Crystallographic Diffraction Database) crystallographic database PDF-4+ (2019 edition). Before analysing all not room temperature (26 °C), written down X-rays 2Θ corner corrections were entered according to quartz diffraction peaks, as in, 2Θ corners were raised so that X-ray quartz peaks would match with PDF-4+ database quartz card's #00-046-1045 shown 2Θ corner values.

Figure 5. Image of XRD equipment.

Fibre-cement chemical composition was investigated using the WD-XRF wave dispersion X-ray fluorescence spectroscopy method. The Spectrometer Axios MAX (PANalytical, Malvern Panalytical B.V., Eindhoven, Netherlands) (Figure 6) used was with 4 kW X-ray source with Rh anode. Chemical composition quantitative analysis was done using method without reference using the program equipment, "Omnian" (PANalytical, Netherlands). The spectrometer was calibrated using 16 standard references provided by the manufacturer. The sample was ground and then milled in a rotary mill Pulverisette 6 (FRITSCH, Germany) (wolfram carbide vessel (volume of 80 cubic cm) and eight wolfram carbide spheres), 550 spins per minute, milled for 5 min. A total of 6 g of gotten powder was mixed with 2 g of special pure wax and milled again for 2 min. Tablets of about 3mm thickness and 37 mm in diameter (Figure 7) were pressed from a powder and a wax (20% mass) mixture were pressed using a hydraulic press TP-20 (Herzog, Germany).

Figure 6. Image of spectrometer Axios MAX.

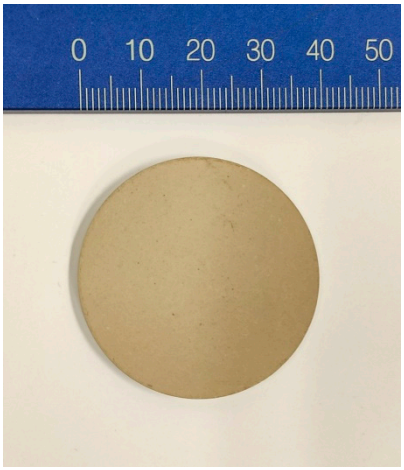

Figure 7. Tablet for XRF investigation.

Macro-structure research was done using optic microscope "Motic" (magnification up to 100 times), characterized zones were photographed using digital camera "Pixera PVC 100C", connected to a computer. Formed samples were cut and photographed using optic microscope (Figure 8) with magnification of 25 times.

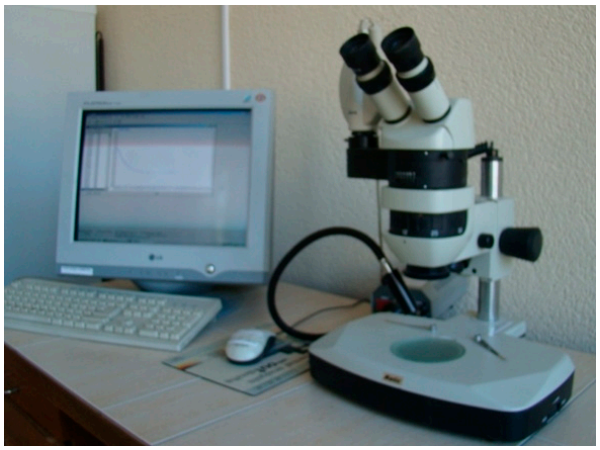

Figure 8. Image of optic microscope "Motic".

3. Results

Fibre-cement plates are binding materials and the product of hydration and hardening of Portland cement, the latter being a matrix that holds bonded aggregates–sand and armouring materials–and cellulose fibres. The hardening process is complicated. According to the various size, form and properties, cement components hydrate at different speeds. Aluminium hydroxide and kaolin are added, and hardening takes place in autoclave conditions.

In normal conditions the reactions of Portland cement minerals with water occur at different rates: C3A reacts the quickest, then C3S and C4AF, while C2S reacts the slowest. Extra hydrates formed during the hydration process react with each other, due to which the final hydrate changes composition [16]. As the cement paste hardens (and in the presence of appropriate temperature) two forms of calcium hydro silicate (CSH) are possible: CSH(I) and CSH(II). It was found that CSH(I) tobermorite gel ($Ca_5Si_6O_{16}(OH)_2 \cdot 4H_2O$) appears at 150 °C. During production the fibre cement plates are affected by temperatures between 120–140 °C; according to the literature data, it is likely that during the production the aforementioned compound forms. After its formation, and exposed to high temperatures, destruction, cleavage and recrystallization reactions occur, as well as other changes. In addition, aggregate, armoured and further destruction takes place.

After investigating fibre-cement X-ray analysis methods (Figure 1) it was determined that at a room temperature of 26 °C, the main phases (excluding quartz, which has been assigned highest peaks in Figure 9) are as follows: $Ca2.93Al1.97(Si_{0.64}O_{2.56})(OH)_{9.44}$ katoite and tobermorite $Ca_{4.5}Si_6O_{15}(OH)_3 \cdot 2H_2O$. Unidentified peaks are revealed under X-ray and this can be attributed to the presence of a large crystal hydrate, which can be identified using a higher optics X-ray diffractometer.

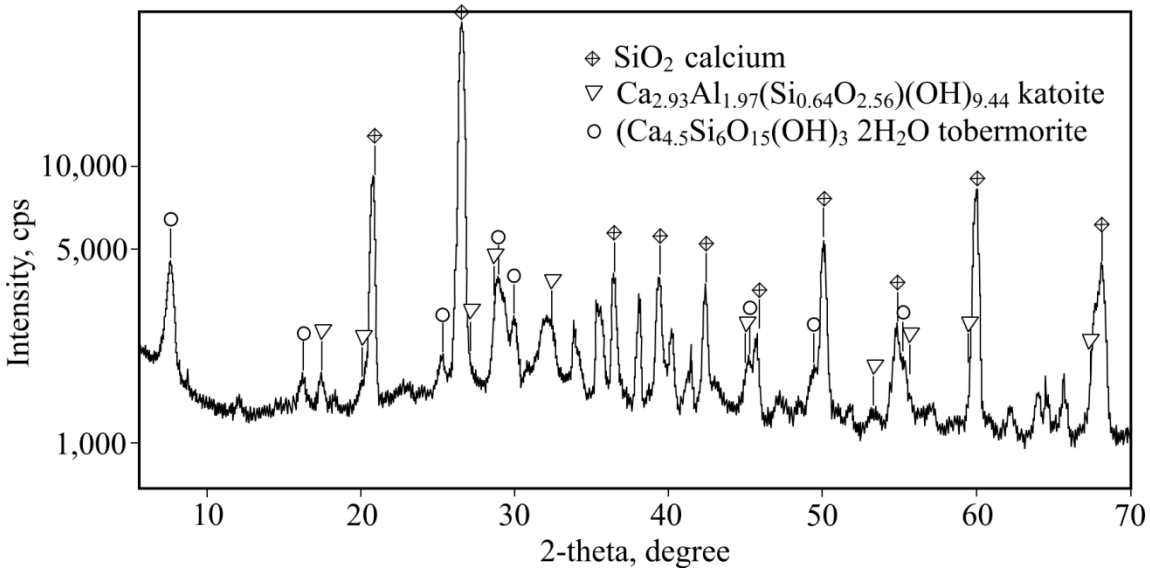

Figure 9. Fibre-cement plate X-ray.

Fibre-cement plate thermogravimetric analysis was performed (Figure 10). After completing multiple investigations, the research results were identical. General mass losses at 1000 °C were 14%. Several endothermic effects were determined that occur at 40–250 °C; 250–390 °C; 390–650 °C; 650–730 °C; 730–1000 °C and which can be explained using the references.

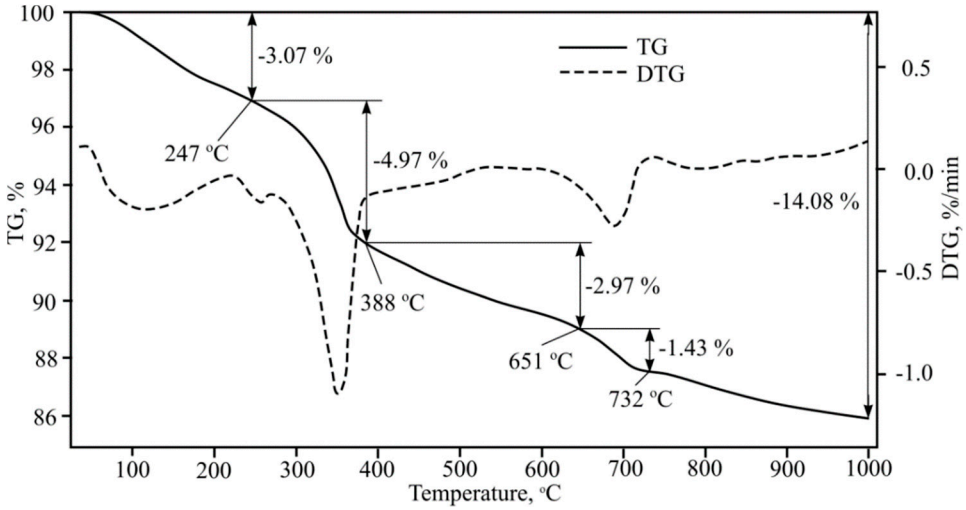

Figure 10. Fibre-cement plate thermogravimetric analysis results: TG–temperature graph; DTG–differential temperature graph.

The endothermic effect at 40–250 °C can be explained first using CSH dehydration; references show that in the stated temperature interval tobermorite changes to xenolite [12]. In these temperatures, gypsum hydrate dehydration takes place, with the formation of alpha form anhydrite. Furthermore, in this temperature interval calcium monosulphate aluminate dehydration formation into crystalline hydrate [20], and hydrated calcium aluminium aminopheritic phase dehydration formation into crystalline hydrate takes place.

Cellulose pyrolysis happens fastest at 250–390 °C afterwards CSH dehydration happens, Al(OH)3 cleavage into boehmite, various calcium aluminium hydrate cleavage (forming other calcium aluminium hydrates, but with a lower chemically bonded water amount), second portlandite forms and during calcium aluminium aminopheritic phase dehydration formed crystalline hydrate cleavage into hydrogrant [21].

In the final dehydration of CSH at temperatures between 390–650 °C, gamma bredigite forms, second portlandite dehydration occurs, and unmalting beta form anhydrite formation takes place. Furthermore, with various calcium aluminium hydrates further cleavage may happen, forming other calcium aluminium hydrates with a lower chemically bonded water amount. Furthermore, hydrogrant cleavage into calcium aluminium hydrate and alpha form hematite occurs. This compound can pass over into the beta form. And, of course, quartz pass over to beta form also occurs.

Metakaolin formation occurs at temperatures between 650–730 °C, Al_2O_3 forms, mayenite ($Ca_{12}Al_{14}O_{33}$) formation from calcium aluminium hydrate, beta hematite changes to gamma form, and calcite dissociation takes place.

At temperatures between 730–1000 °C wollastonite formation, beta form larnite changes into alpha form larnite, gamma bredigite changes to alpha form bredigite, beta form quartz changes to alpha form tridymite and sillimanite, and metakaolin starts to change to cristobalite and mullite.

Composite fibre-cement material component dehydration and cleavage is a complicated process [22]. Endothermic effects overlap when performing thermogravimetric analysis in such composite material like fibre-cement, due to this separate composite material thermogravimetric analysis was done. Kaolin, two cellulose types and aluminium hydroxide were separately investigated. Cement thermogravimetric analysis results are not shown due to the fact that cement powder in mixture when mixed with water hydrates and practically completely changes into new compounds. Quartz sand thermogravimetric analysis is not performed due to the fact that differential thermal analysis method is needed to determine entropic polymorphism.

No changes take place related to mass loss when heating only quartz sand, and thermal effects are also not observed. Sand constitutes up to 51% of fibre-cement mass. Differently from cement concrete, hardened in natural conditions, quartz sand surface in fibre-cement takes part in hydration and hardening processes during autoclave conditions. Calcium hydro silicates are formed due to these processes [23]. This means that fine sand forms part of the reactions and forms new compounds, while coarse sand plays the role of framework in the composite. The best case scenario is that it can only be hydrated with the surface of this sand.

Narrow peaks of the smaller size towards quartz peaks become visible when fibre-cement is heated to 1000 °C and the quartz component is investigated (Figure 11). These peaks accord well with silica X SiO_2 or High quartz peaks and form at ~600 °C with a deformed quartz lattice system which indicates the presence of impure quartz.

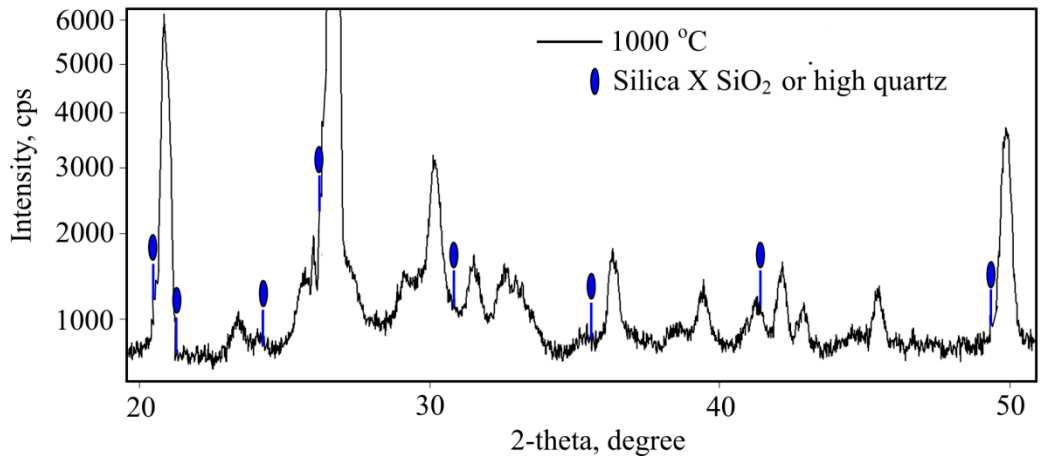

Figure 11. Quartz X-ray at 1000 °C.

The armouring added to fibre-cement is filled by cellulose fibres, with two types (shorter and longer) being used in plates which are spread into a "hand fan" during mass mixing. Thermogravimetric analysis results for longer cellulose fibre are shown in Figure 12.

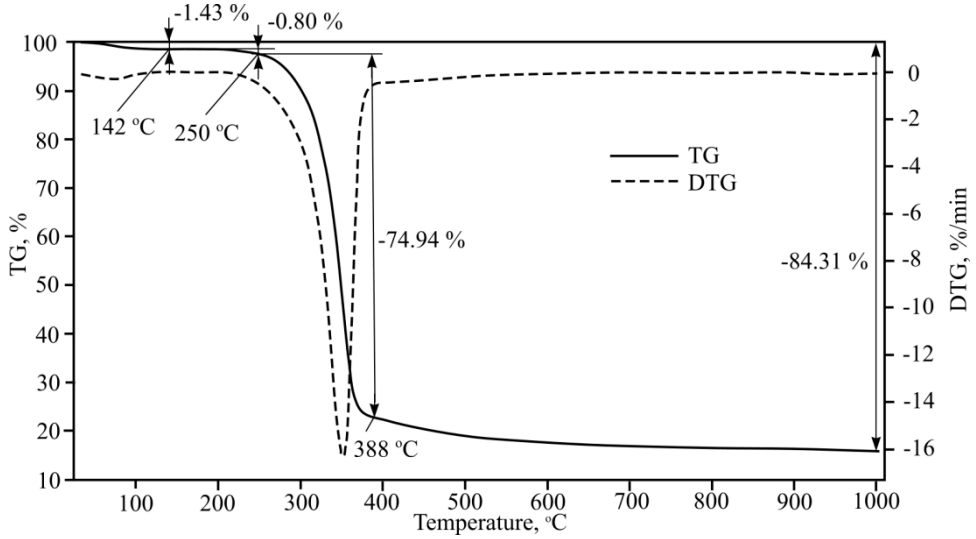

Figure 12. First type cellulose fibre thermogravimetric analysis results: TG–temperature graph; DTG–differential temperature graph.

According to data shown in the figure, one clear endothermal effect is observed when heating this cellulose fibre type. Cellulose pyrolysis starts at 250–256 °C, with the main and intensive mass loss taking place up to 388 °C at which point 75% mass is lost. Due to the link destruction of C-C, C-O levoglucosan forms in cellulose and its further thermal cleavage happens near 600 °C. At higher temperatures, the line flattens even though 3,6-anhydrate-D-glucose and 1,4:3,6-dianhydrate-D-glucose formation is taking place [24].

Thermogravimetric analysis results for shorter cellulose fibre are shown in Figure 13.

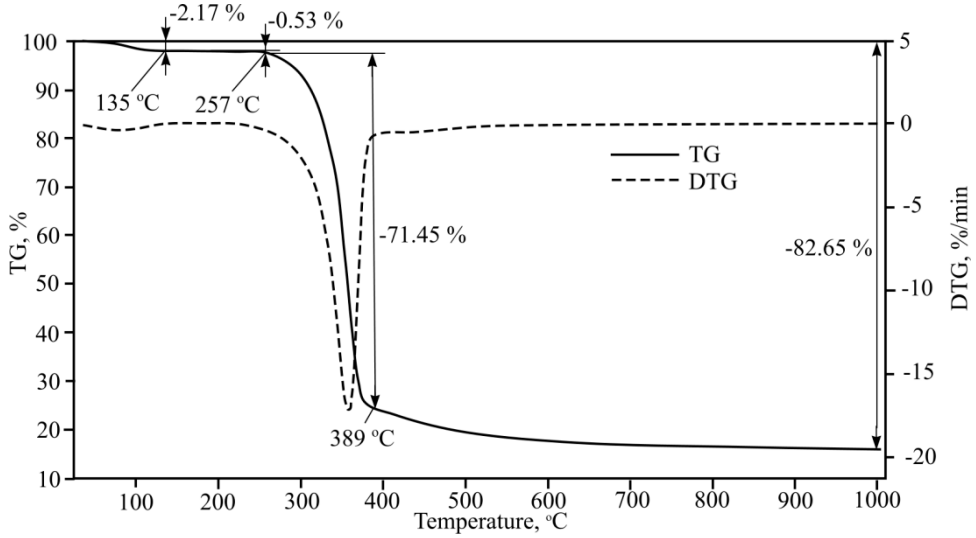

Figure 13. Second type short cellulose fibre thermogravimetric analysis results: TG–temperature graph; DTG–differential temperature graph.

One clear endothermic effect was observed with 71.45% mass loss occurring from 389 °C when heating second type cellulose. During fibre-cement plate production cellulose fibre reacts with hydrated Portland cement and other components. Physical, chemical and mixed bonds form between cellulose and cement matrixes, however, despite bonds forming between the materials that influence general mechanical composition strength, one of the evident endothermic effects is due to cellulose destruction when fibre-cement is heated. If we were to calculate cellulose mass percentage in fibre-cement, then about 5%–6% mass loss would be suffered due to cellulose destruction and

pyrolysis. This is confirmed by cellulose X-ray phase analysis performed at 26, 110, 220, and 400 °C (Figure 14).

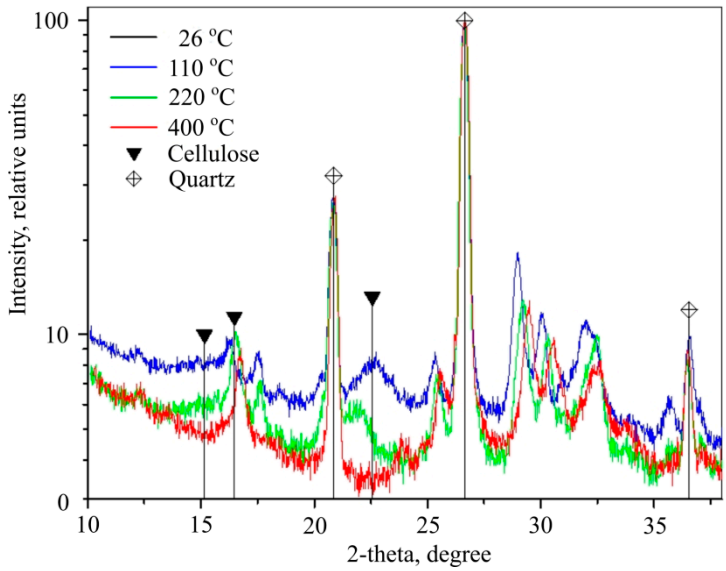

Figure 14. Cellulose X-ray phase analysis results.

X-rays taken during 26 °C and 110 °C almost completely match, due to which the first (the one coloured black) is not visible. Black triangles show wide, yet small intensity peaks at 2Θ corners 15.16, 16.48 and 22.57°, which are attributed to cellulose $C_6H_{10}O_5n$. These peaks are shown at 110 and 220 °C in X-rays (black and white, respectively), but are not visible at 400 °C measured X-ray (red). Therefore, cellulose should disintegrate in temperatures from 220 °C and 400 °C. According to [25] fibre-cellulose incinerates and disintegrates at 328 °C.

The structure of the plate was also investigated using optic microscope. Firstly, the pictures of the plates' structure were taken, and then the plate was burned in 1000 °C temperature. After the burning, the picture of the plate was taken using the same magnification. Pictures of plate's natural status and post-burning are shown in Figure 15. After temperature effect takes place we can observe that there are no cellulose fibres left. They have burned off; the only thing left is the cement structure repeating the previous fibre view.

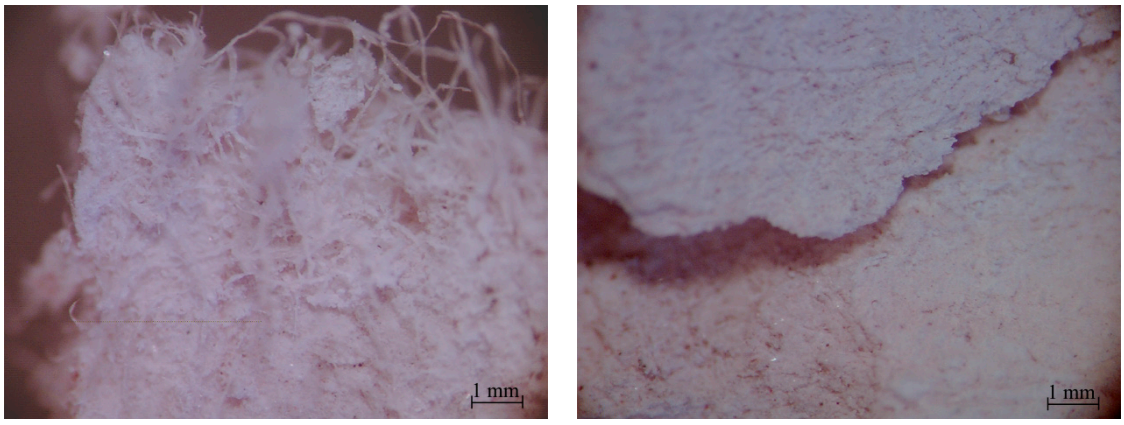

(**a**) (**b**)

Figure 15. Structure of the plate: (**a**) plate in natural status and (**b**) after burning in 1000 °C temperature (on the right) magnification–25 times.

Aluminium hydroxide $Al(OH)_3$ is used as an addition to improve fibre-cement plate final properties. Aluminium hydroxide thermogravimetric analysis results are shown in Figure 16.

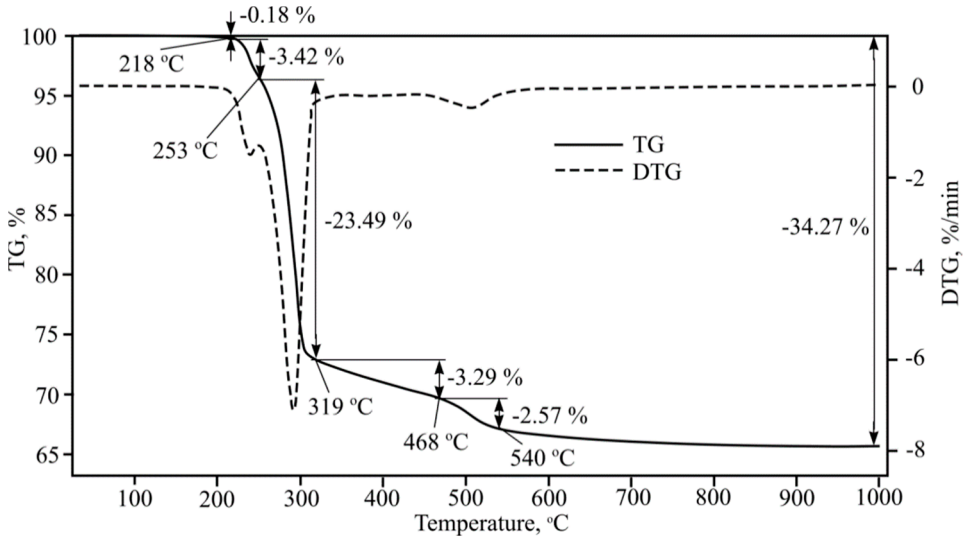

Figure 16. Aluminium hydroxide thermogravimetric analysis results: TG–temperature graph; DTG–differential temperature graph.

Figure 16 shows that aluminium hydroxide in fibre-cement changes into other compounds. One study [26] determined that aluminium hydroxide $Al(OH)_3$ during the hydration process of Portland cement reacts with other components and creates compound ettringite $6CaO{\cdot}Al_2O_3{\cdot}3SO_3{\cdot}32H_2O$, which slows cement hydration. After a certain period of time, this compound transforms into another compound, i.e., calcium monosulphate aluminate $4CaO{\cdot}Al_2O_3{\cdot}SO_3{\cdot}12H_2O$, and water molecule blockage breaks off. It was determined that aluminium hydroxide $Al(OH)_3$ usage in regular cement products provides the same resistance to fire characteristics as aluminate cement with 40% Al_2O_3 amount. Another study performed aluminate cement X-ray and thermal analysis, during which tricalcium aluminate 6-hydrate $3CaO{\cdot}Al_2O_3{\cdot}6H_2O$ and gypsum $Al_2O_3{\cdot}H_2O$ dehydration temperatures were determined, which were 314–322 °C and 293–294 °C, respectively. During the gypsum $Al_2O_3{\cdot}H_2O$ thermal cleavage process, boehmite γ- $Al_2O_3{\cdot}H_2O$ forms which completely dehydrates near 700 °C into amorphous Al_2O_3. In Figure 1, the endothermic effect that take place at 700 °C can be seen.

Kaolin is added to fibre-cement plate formation mass mixture. Kaolin thermogravimetric analysis results are shown in Figure 17.

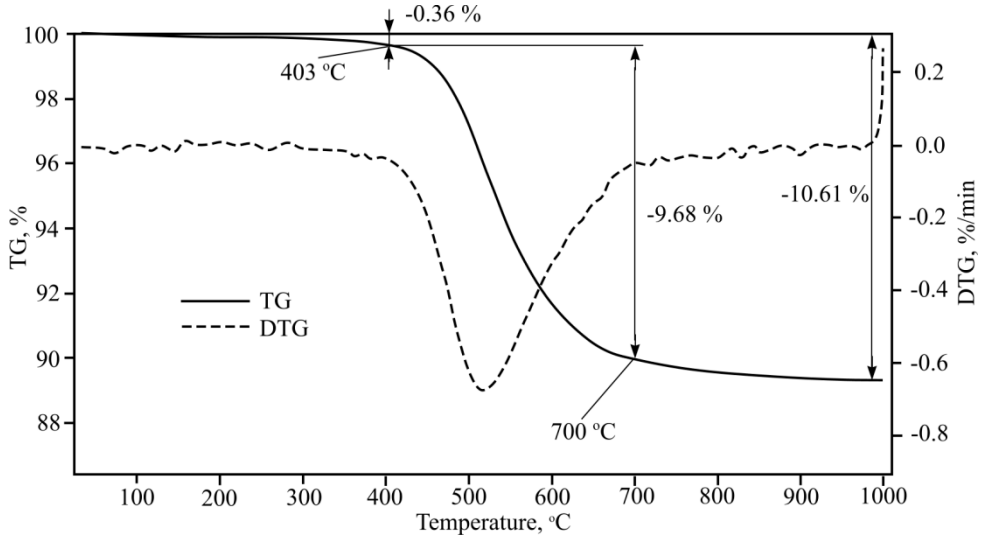

Figure 17. Kaolin thermogravimetric analysis results: TG–temperature graph; DTG–differential temperature graph.

The behaviour of kaolin $Al_2O_3 \cdot 2SiO_2 \cdot 2H_2O$ at high temperatures [27]: first, at 100–250 °C absorbed water withdrawal takes place, while at 350–600 °C interval bonded water withdrawal occurs. The endothermic effect due to structural change is fixated at 520–635 °C. First phase change is determined at 600–800 °C, when metakaolin $Al_2O_3 \cdot 2SiO_2$ forms. At 700–1000 °C, water withdrawal and metakaolin formation ends. A clear exothermic reaction is fixated at 920–940 °C when amorphous Al_2O_3 changes into γ-Al_2O_3 form. Previous research [28] indicates that at 925–1050 °C amorphous SiO_2, cristobalite, separation happens. When the temperature reaches 950–1200 °C metakaolin completely cleaves and sillimanite, cristobalite and mullite form.

X-rays were taken while heating fibre-cement during the mass heating process from 26 °C to 1000 °C (Figure 18). The X-rays revealed main minerals including, quartz, tobermorite, katoite, wollastonite, akermanite, mullite, and cellulose. Quartz is visible in all X-rays. Cellulose peaks disappear when the temperature reaches 400 °C. In low temperatures tobermorite peaks are visible as well as katoite peaks. In high temperatures other compounds are observed: wollastonite, akermanite and mullite.

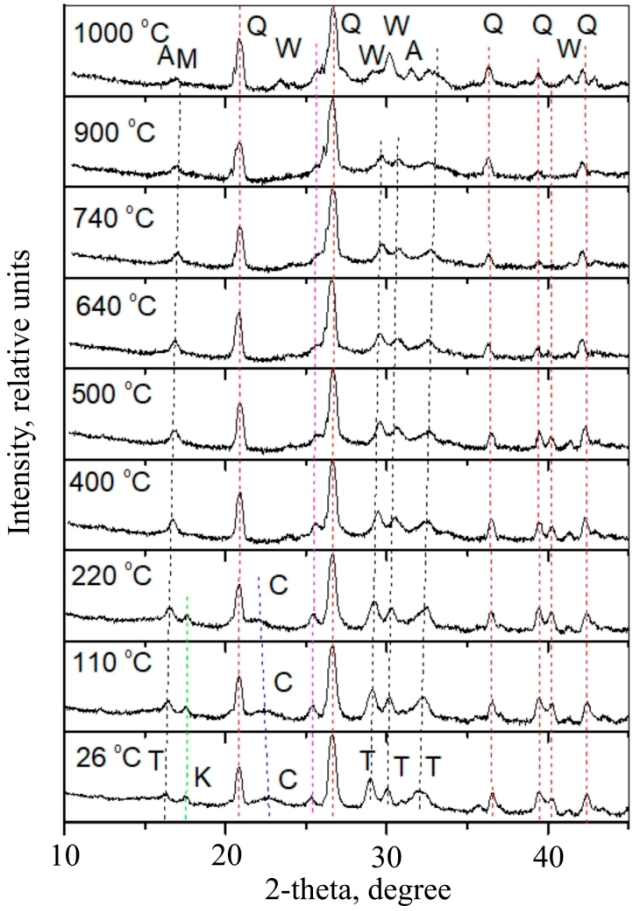

Figure 18. Fibre-cement X-ray phase analysis results in 26-1000 °C temperature: Q–quartz; T–tobermorite; W–wollastonite; C–cellulose; M–mullite; K–katoite; A–akermanite.

Peaks appear in X-rays when temperatures rise in 640–900 °C intervals, but without quartz peaks that can be attributed to $CaSiO_3$ calcio-olivine (Figure 19). After reaching 1000 °C (Figure 19) quartz remains in the main phase, while olivine turns into wollastonite ($CaSiO_3$), which can also be another form of wollastonite $(Ca,Fe)SiO_3$ that contains iron. Here, peaks can be attributed to compound $Ca_2Mg_{0.5}Al_{0.92}Si_{1.54}O_7$.

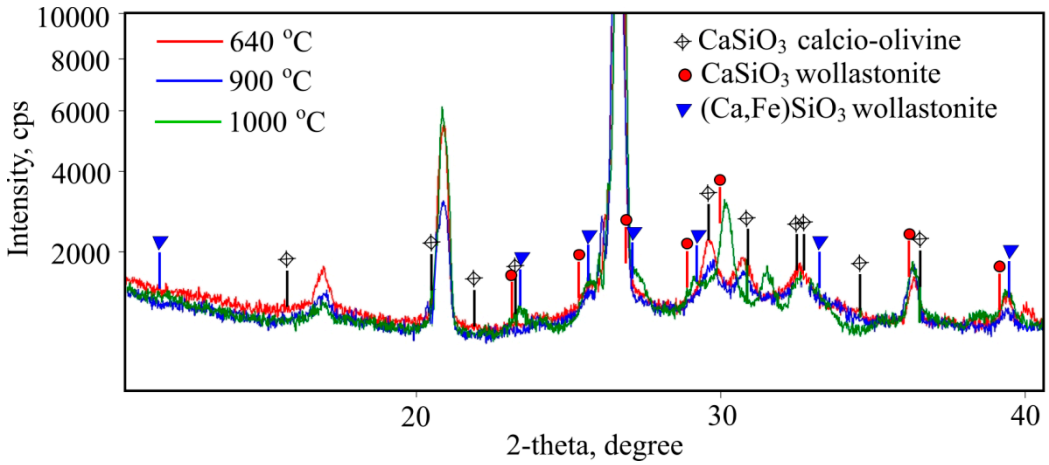

Figure 19. Fibre-cement X-ray phase analysis results in 640 °C, 900 °C and 1000 °C temperatures.

According to the methodology applied to the first and second formulas, two different temperature fibre-cement plate heating regimes were chosen, taking into account standard fire curves (Figure 20). According to the first formula, heating of the fibre-cement was performed in regimes from 35 °C to 680 °C, while the temperature rise speed was chosen according to the external fire curve [29,30], which is shown in the methodological part. Other temperature regimes were from 35 °C to 842 °C, and rise speed was chosen according to the standard (interior) fire curve.

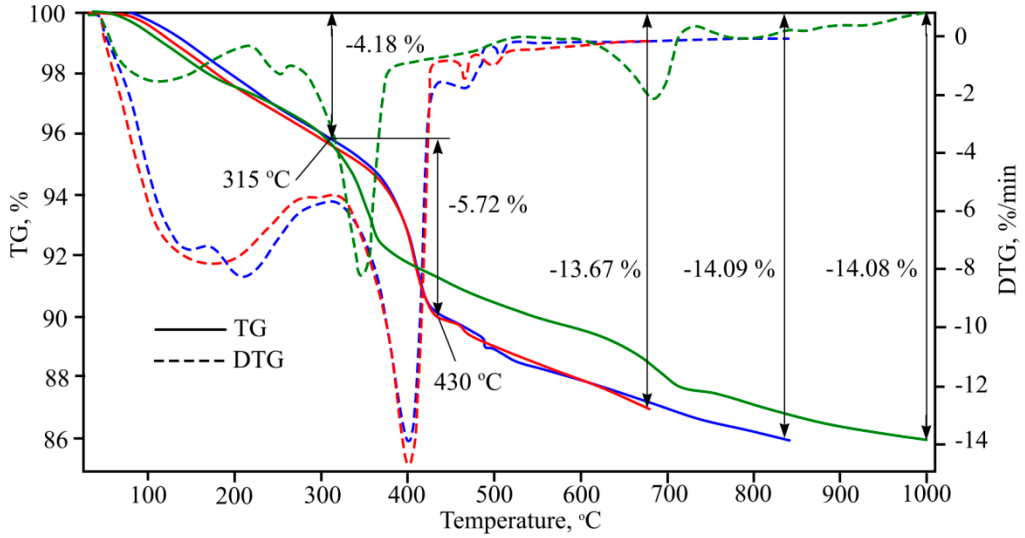

Figure 20. Fibre-cement plate thermogravimetric analysis results: red curve–heating according external fire curve; blue curve–heating according to Standard (interior) fire curve; green curve–heating at 10 °C/min speed; TG–temperature graph; DTG–differential temperature graph.

As the heating speed changes, the intensity of the endothermic effect also changes. Thus, when heating is more intensive, the processes taking place during the heating are more intensive. Furthermore, the endothermic effect disappears at 650–730 °C. When mass losses are compared, the more intensive the heating regime, results in higher mass losses. Whilst the difference is not significant, it is visible. After analysing all three TG curves it can observed that up to 315 °C mass is lost, after which the curves separate. According to the green curve, mass lowers more intensively up to 360 °C, after which mass loss becomes stable up to endothermic effect at 650–730 °C. According to the blue and red TG curves, mass falls suddenly at 380 °C temperature and continues until 430 °C. After this point mass lowers gradually, while the sudden mass loss determines higher final mass difference.

4. Discussion

After completing the research described herein, and investigating the processes that take place in fibre-cement during heating, it is clear that to properly address the problem raised (cleavage of the fibre-cement plate during a fire), further investigation is required in what kind of processes take place in these products when they are used in an environment that is completely different from the standard research environment. This article shows what compounds form during standard research conditions and also raises hypotheses using information from references [19–21,25,27]. It should be noted that in real fire conditions information, which is shown in one or another reference, is not always applicable; in the case of fire, research and experiment conditions must align more closely with those found in non-standard situations. Further, when a fibre cement product is burned, the composition of such a product may contain various chemical compounds which can in one or another way aggressively erode the structure of the fibre-cement [31] in parallel thermal destruction. These circumstances were not taken into account during this research.

5. Conclusions

Autoclave mass hardening is used when producing fibre-cement, during which one of the CSH phases forms (calcium silicate hydroxide hydrate) which is a mineral in the tobermorite group. This compound has a thin-layered fibre-cement plate base, while plates are strengthened using cellulose fibres. The chemical composition of main fibre-cement plate consists of oxides of silicon and calcium.

When fibre-cement plates are heated at 1000 °C, the general loss of mass is 14%. Determined endothermic effects occur at temperatures of 40–250 °C; 250–390 °C; 390–650 °C; 650–730 °C; and 730–1000 °C.

Individual cellulose fibre thermograms and X-rays show that cellulose fibres burn at temperatures of up to 400 °C while the determined endothermic effects end at 389 °C with mass loss of 71%–75%, depending on the type of cellulose used for armouring.

During the heating of fibre-cement, the following composition minerals and their phase changes take place: at 26 °C calcium silicate hydroxide hydrate (a mineral in the tobermorite group which composes the plate's base), with katoite changes into volastonite, acermanite, and mullite. The main phases of the aforementioned are determined at 1000 °C.

When heating parameters are changed for fibre-cement plates, the intensity of the processes taking place during a fire also changes. This may help to explain why fibre-cement plate cleavage and explosive disintegration appears.

During research transformation and dehydration dynamic was determined which shows critical temperature boundaries for different components. These results grant information when trying to improve fire resistant fibre-cement product properties and choosing extra components and their amounts. Special attention should be paid to cellulose fibre destruction temperatures. The thermal destruction of this component happens in rather low temperatures according to fire curves [27]. Cellulose fibre and cement matrixes bond destruction determines the whole products destruction. However, these same bonds are important for ensuring other fibre-cement plates properties quality. Due to this, more detailed research is relevant for the elimination or reduction of this process without influencing the main fibre-cement plate properties [2].

Further research is needed in X-ray analysis using a more sensitive optic and also in other gas environments in order to produce a more detailed fibre-cement thermal change analysis, and to confirm or challenge changes described in references.

Author Contributions: Conceptualization, R.Z., T.V. and M.V.; methodology, R.Z.; software, R.Z.; validation, T.V., M.V., and R.Z.; formal analysis, T.V., R.Z.; investigation, T.V. and R.Z.; resources, M.V.; data curation, T.V. and R.Z.; writing—original draft preparation, T.V. and M.V.; writing—review and editing, R.Z., M.V. and T.V.; visualization, R.Z. and T.V.; supervision, R.Z. and M.V.; project administration, R.Z.; funding acquisition, R.Z. All authors have read and agreed to the published version of the manuscript.

Funding: This research received no external funding.

Acknowledgments: The authors express their appreciation for the significant editing contribution of English-born Ron Ringer, a professional writer and author of numerous publications and the NGO, Materials users and producers association, a professional team and authors of numerous publications from Vilnius (Lithuania).

Conflicts of Interest: The authors declare no conflict of interest.

References

1. Callister, W.D. *Materials Science and Engineering*: *An Introduction*, 7th ed.; Wiley: New York, NY, USA, 2007.
2. *EN 12467:2012+A2:2018 Fibre-cement Flat Sheets. Product Specification and Test Methods. LST EN 12467:2012+A2:2018 Lt*; Lithuanian Standard Board: Vilnius, Lithuania, 2018.
3. Gorzelanczyk, T.; Schabowicz, K. Nondestructive Testing of Moisture in Cellulose Fiber Cement Boards, In Proceedings of the 11th European Conference on Non-Destructive Testing, Prague, Czech Republic, 6–10 October 2014.
4. Brushlinsky, N.N.; Hall, J.R.; Sokolov, S.V.; Wagner P. World fire statistics. *Cent. Fire Stat. CTIF* **2018**, *10*, 1-31..
5. Kotthoff, I.; Riemesch-Speer, J. Mechanism of fire spread on facades and the new Technical Report of EOTA "Large-scale fire performance testing of external wall cladding systems". *MATEC Web Conf.* **2013**, *9*, 02010, doi:10.1051/matecconf/20130902010.
6. Bong, F.N.P. Fire Spread on Exterior Walls. Master's Thesis, University of Canterbury, Christchurch, New Zealand, 2000.
7. Rukavina, M.J.; Carevic, M.; Pecur, I.B. Fire protection of facades. In *The Guidelines for Designers, Architects, Engineers and Fire Experts*; University of Zagreb: Zagreb, Croatia, 2017; p. 64.
8. Kuzyk, A.; Yakovchuk, R.; Yemelyanenko, S. FDS simulation of fire spread EPS insulated facade and comparison of model results with experimental data. *News Natl. Acad. Sci. Repub. Kazakhstan Ser. Geol. Tech. Sci.* **2020**, *18*, 45-48.
9. Jansson, R. Fire Spalling of Concrete: Theoretical and Experimental Studies. Ph.D. Thesis, KTH Royal Institute of Technology, Stockholm, Sweden, 2013.
10. Hertz, K. The anchorage capacity of reinforcing bars at normal and high temperatures. *Mag. Concr. Res.* **1982**, *34*, 213–220.
11. Phan, L.T.; Carino, N.J. Review of Mechanical Properties of HSC at Elevated Temperature. *J. Mater. Civ. Eng.* **1998**, *10*, 58–65.
12. Kosmatka, S.H.; Kerkhoff, B.; Panarese, W.C. *Design and Control of Concrete Mixtures*, 4th ed.; Portland Cement Association: Illinois, Portland, 2003; p. 370.
13. Štefan, R.; Foglar, M.; Fládr, J.; Horníková, K.; Holan, J. Thermal, spalling, and mechanical behaviour of various types of cementitious composites exposed to fire: Experimental and numerical analysis. *Constr. Build. Mater.* **2020**, *262*, 119676, doi:10.1016/j.conbuildmat.2020.119676.
14. Antonovič, V.; Witek, J.; Mačiulaitis, R.; Boris, R.; Stonys, R. The effect of carbon and polypropylene fibers on thermal shock resistance of the refractory castable. *J. Civ. Eng. Manag.* **2017**, *23*, 672–678.
15. Peng, G.-F.; Niu, X.-J.; Shang, Y.-J.; Zhang, D.-P.; Chen, X.-W.; Ding, H. Combined curing as a novel approach to improve resistance of ultra-high performance concrete to explosive spalling under high temperature and its mechanical properties. *Cem. Concr. Res.* **2018**, *109*, 147–158.
16. Veliseičik, T.; Šarauskas, T.; Lazdauskas, L.; Guoga, E. The research of fire impact for reveal of external thermal insulation composite system with rendering. *Sci. Future Lith.* **2020**, *12*, 1–6.
17. Abzaev, A.Y.; Gnyrya, I.A.; Korobkov, S.; Gauss, K.S. Phase analysis of hydrated Portland cement. *IOP Conf. Ser. Earth Environ. Sci.* **2018**, *193*, 012001, doi:10.1088/1755-1315/193/1/012001.
18. Taylor, H.F.W. Tobermorite, jennite, and cement gel. *Cryst. Mater.* **2015**, *202*, 1–4.
19. Hager, I. Behaviour of cement concrete at high temperature. *Bull. Pol. Acad. Sci. Tech. Sci.* **2013**, *61*, 145–154.
20. Maier, M.; Zeiml, M.; Lackner, R. On the effect of pore-space properties and water saturation on explosive spalling of fire-loaded concrete. *Constr. Build. Mater.* **2020**, *231*, 117150, doi:10.1016/j.conbuildmat.2019.117150.
21. Shaw, S.; Henderson, C.M.B.; Komanschek, B. Dehydration/recrystallization mechanisms, energetics, and kinetics of hydrated calcium silicate minerals: An in situ TGA/DSC and synchrotron radiation SAXS/WAXS study. *Chem. Geol.* **2000**, *167*, 141–159.

22. Zhu, B.; Fang, B.; Li, X. Dehydration reactions and kinetic parameters of gibbsite. *Ceram. Int.* **2010**, *36*, 2493–2498.
23. Antonovič, V. Influence of Sodium Silicate and its Solution on the Properties of Refractory Concrete (in Lithuanian Natrio silikato ir jo tirpalo įtaka kaitriai atsparaus betono savybėms). Ph.D. Thesis, Vilnius Gediminas Technical University, Vilnius, Lithuania, 1999.
24. Nimlos, R.M.; Evans, R.J. Legoglucosan pyrolysis. *Fuel Chem. Div. Prepr.* **2002**; *47*, 393–394.
25. Liping, G.; Wenxiao, Z.; Wei, S.; Bo, C.; Yafan, L. High-Temperature Performance and Multiscale Damage Mechanisms of Hollow Cellulose Fiber-Reinforced Concrete. *Adv. Mater. Sci. Eng.* **2015**, *2016*, doi:10.1155/2016/2503780.
26. Brykov, A.S.; Vasil'Ev, A.S.; Mokeev, M.V. Hydration of Portland cement in the presence of high activity aluminum hydroxides. *Russ. J. Appl. Chem.* **2012**, *85*, 1793–1799.
27. Kazragis, A.; Valaitytė, L.; Juknevičiūtė, A. Thermodynamics of high-temperature interaction of gypsum and kaolin. Modern building materials, structures and techniques. In Proceedings of the 7th International Conference, Vilnius, Lithuania, 16–18 May 2001.
28. Ptáček, P.; Šoukal, F.; Opravil, T.; Havlica, J.; Brandštetr, J. The kinetic analysis of the thermal decomposition of kaolinite by DTG technique. *Powder Technol.* **2011**, *208*, 20–25.
29. *Eurocode 1: Actionns on Structures—Part 1–2: General Actions—Actions on Structures Exposed to Fire: LST EN 1991-1-2:2004 Lt*; Lithuanian Standard Board: Vilnius, Lithuania, 2004.
30. *ISO 13785-1 Reaction-to-Fire Tests for Facades—Part 1: Intermediate-Scale Test. LST ISO 13785:2016 Lt*; Lithuanian Standard Board: Vilnius, Lithuania, 2016.
31. Cooke, A.M. Durability of Autoclaved Cellulose Fiber Cement Composites. In Proceedings of the 7th Inorganic-Bonded Wood and Fiber Conference, 15–17 October 2000.